Applying an Unfolding Method with Monte Carlo Simulations of IceCube Electron (anti-)Neutrinos induced Cascade Data

Colton Addis
Dr. Joanna Kiryluk, Dr. Zelong Zhang, Zheyang Chen

Iowa State University of Science and Technology

Stony Brook University

Abstract

IceCube Neutrino Observatory is a cubic kilometer detector located at the South Pole in Antarctica. In this project we will utilize Monte Carlo Pass2 high energy neutrino induced cascade data, re-optimize energy and zenith binning and study unfolding of true electron (anti-)neutrino kinematic variables. The neutrino Monte Carlo generators used in NuGen, studies comparing to Lepton Injector are in progess.

Introduction

- IceCube is a km^3 of ice in Antartica, with 5160 optical modules [1] used as a neutrino telescope.
- It detects Cherenkov light produced when a neutrino interacts with quarks and antiquarks in the target nucleons.
- There is a systematic source of error from the process of reconstructing the energy and direction of neutrino from Cherenkov light.
- To recover true variables from these reconstructed ones, unfolding is used.

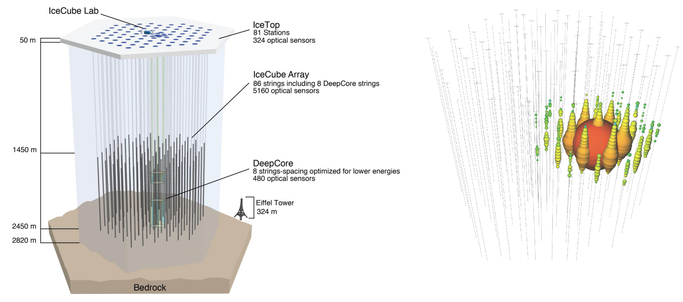

Credit: IceCube Collaboration

Unfolding

- Unfolding is a process that takes a distribution of reconstructed data and finds the true distribution from that and needs an unfolding matrix.
- To create an unfolding matrix, Monte Carlo simulations of events are used where both true and reconstructed values are known.
- The unfolding matrix is the probability an event in a reconstructed bin is in some true bin.
- Below is an unfolding test with toy data, with the data sampled from 3 normal distributions and a unform background.

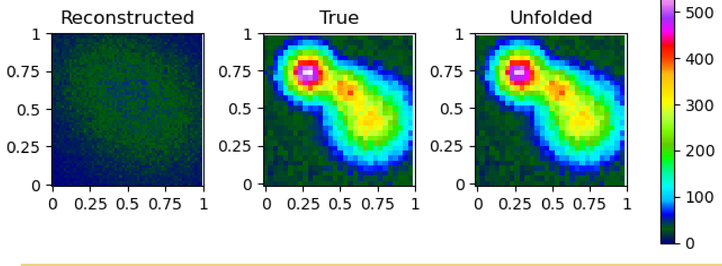

Figure 1: A test of the Richardson-Lucy unfolding algorithm with toy data. The reconstructed data has an assumed resolution of 0.25 and no bias. 100 iterations was used for the unfolding algorithm. The reconstructed data is in 60 x 60 bins, and the true and unfolded data is in 30 x 30 bins.

The Unfolding Algorithm

- The Richardson-Lucy unfolding algorithm [2] is used.
- The unfolding matrix (A) is created from the probability a value in a true bin j is in some reconstructed bin i.
- It starts with a guess of the true distribution, then in iterations makes an estimate of the reconstructed distribution (d_i) from the current unfolded distribution ($\hat{\theta}_j$ and the unfolding matrix.
- Each iteration the algorithm attempts to minimize the difference between the estimate and unfolded distributions.
- α is a vector that represents the acceptance loss when making the unfolding matrix.

$$d_i^{(k)} = \sum_{j=1}^{N} A_{ij}\hat{\theta}_j^{(k)} \quad . \qquad \hat{\theta}_j^{(k+1)} = \sum_{i=1}^{M} A_{ij}\hat{\theta}_j^{(k)} \frac{d_i}{d_i^{(k)}} / \alpha_j \quad .$$

Binning Optimization

- The parameters of interest are the energy of the neutrino and zenith angle. They are unfolded together as a 2D histogram, with log(E) as the x-axis and cos(Z) as the y-axis.
- A bin width of .2 was chosen for log(E), corresponding to 22 bins
- A bin width of .5, or 4 bins, was chosen for cos(Z)
- This was done by looking at the resolution of the reconstructed data, and by looking at the minimum number of events for the bins on the edge of the histogram.
- The graph on the right shows the energy data binned, with a timespan of 11 years, as it is for unfolding.

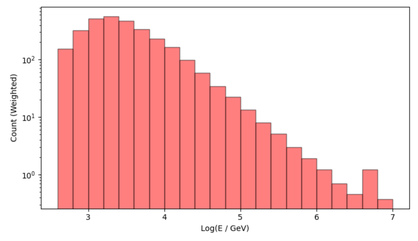

Results on NuGen Monte Carlo Simulated IceCube Data

- Using optimized number of bins and iterations, the result is below.
- A timespan of 11 years was used when weighting.
- The results were tested against a χ^2 distribution and a good agreement was found.

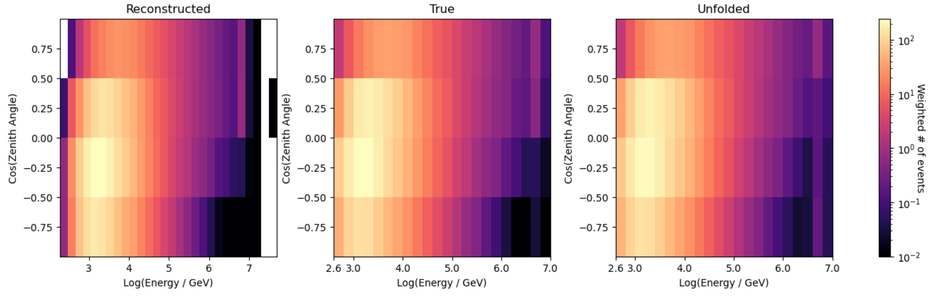

Figure 2: The final results of unfolding the Monte Carlo simulated data. The bin width here is .2 for log(E) space, and .5 for cos(Z) space. 4 iterations of the unfolding algorithm were run.

Optimizing Unfolding Iterations

The number of iterations with a small bias, which decreases through iterations, and a small variance, which increases through iterations, needs to be found. To do this, a log-likelihood ratio is used to estimate the bias from the reconstructed values, because the true values are unknown [3]. The difference between the reconstructed and unfolded is found, and when the log-likelihood passes a critical value the iterations are stopped. To get the critical value, a Poisson sample is taken from the reconstructed 100,000 times, and the log-likelihood is found for each time. When the log-likelihood passes half of that distribution, where p = 0.5, double the iterations is run. This results in 4 iterations being run when used on the simulated data.

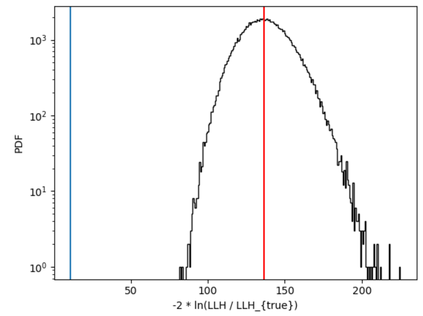

Figure 3: Graphing showing sampling log-likelihood ratio (black), and the log-likelihood ratio of the unfolding after 2 iterations. Since the unfolding is past the critical value (red), the algorithm will run double the iterations and stop

Discussion/Conclusion

- The unfolding algorithm takes a reconstructed distribution and finds the true distribution associated with it.
- To create the unfolding matrix, NuGen Monte Carlo simulations where the true values are known were used. Studies with Lepton Injector are in progress.
- Bin sizes were found by looking at resolution and minimum statistics.
- Iterations count was found from log-likelihood ratios minimizing bias while keeping variance low.
- Future work could be done to implement error analysis when unfolding.
- The algorithm could also be tested with different flavors of neutrinos.

References

[1] F. Halzen, S.R. Klein, IceCube: An Instrument for Neutrino Astronomy, (2010) . https://doi.org/10.48550/arXiv.1007.1247.
[2] G. Zech, Iterative unfolding with the Richardson-Lucy algorithm, (2013). https://doi.org/10.48550/arXiv.1210.5177.
[3] Y. Xu, Measurement of the High Energy Neutrino-Nucleon Cross Section Using Neutrino-Induced Electromagnetic and Hadronic Showers Observed in Five Years of IceCube Data (2019)

Acknowledgements

Thanks to IceCube Stony Brook Group for data and support, and thanks to my mentor, Dr. Kiryluk

NSF | IceCube Neutrino Observatory

Cosmic Ray Muon Flux

Ryan Palumbo, Purdue University

hpDIRC at ePIC

The **Electron-Ion Collider (EIC)** is a next-generation collider being built at BNL to study the quark and gluon structure of matter.

The **hpDIRC** (high-precision Detection of Internally Reflected Cherenkov light) is a compact Cherenkov detector that identifies charged hadrons and muons by imaging Cherenkov photons (their unique Cherenkov ring) produced in synthetic fused silica bars.

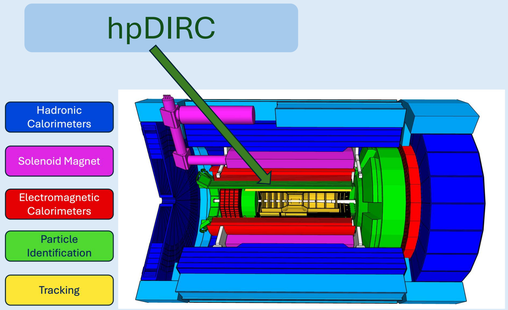

*Images obtained from epic-eic.org and researchgate.net

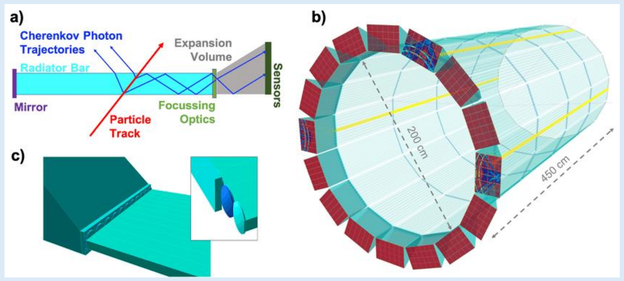

a) Cross-section of hpDIRC in action
b) Proposed setup; long bars in cylindrical shape
c) Connection point between fused silica and expansion volume

Cosmic Ray Muons and the CRT

Cosmic muons are high-energy particles produced in the atmosphere that reach Earth's surface at a steady rate. Muons don't interact much with most matter and have long lifetimes; at the EIC, they provide a convenient calibration source for detectors like the hpDIRC for both detector validation and future data correction in **ePIC**.

The **cosmic ray telescope (CRT)** detects and reconstructs cosmic muon trajectories, providing precise timing and position data to calibrate and conduct performance validation of the hpDIRC detector.

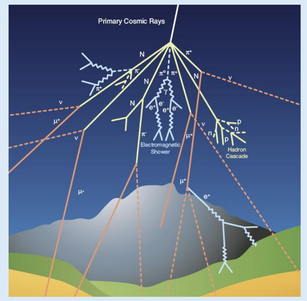

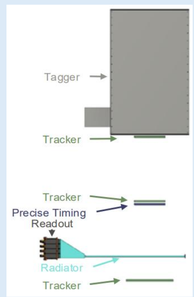

*Images obtained from home.cern and jlab.org

Calculations & Simulation

Theoretical calculations and Monte Carlo (and other) simulations using the **CRY** cosmic ray generator model muon flux and trajectories through the detector setup. These simulations also calculate solid angle and muon flux, supporting design optimization and interpretation of experimental data for precise calibration of the hpDIRC.

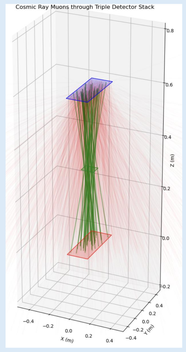

Theoretical flux calculated using Gaisser Parameterization:

$$\frac{dN}{dE_\mu dA dt d\Omega} = 0.14 \cdot \left(\frac{E_\mu}{GeV}\right)^{-2.7} \cdot \left(\frac{1}{1+\frac{1.1E_\mu cos\theta}{115GeV}} + \frac{0.054}{1+\frac{1.1E_\mu cos\theta}{850GeV}}\right)$$

Expected muon flux from cosmic rays at sea level:

$$\Phi_\mu = 167 \pm 0.3 m^{-2}s^{-1}$$

Simulated & calculated solid angle: $\Omega = 0.62sr$

Simulated muon flux: $\Phi_\mu = 160 \pm 13 m^{-2}s^{-1}$

*Image generated by my code in Python

Experiment & Conclusion

We used a mini Cosmic Ray Telescope (mini-CRT) consisting of stacked scintillators coupled to photomultiplier tubes (PMTs) to measure the flux of cosmic muons at the detector site. By varying the high-voltage supply to the PMTs, we found an optimal operating range maximizing muon signal detection while suppressing background noise. Triple-coincidence logic between scintillator ensured event validity.

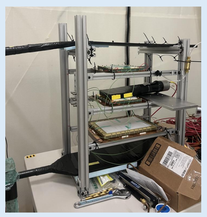

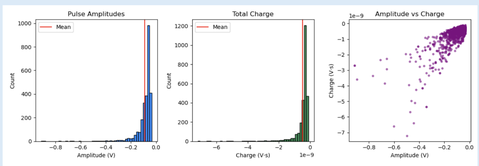

*Images taken or generated by myself or my code

Experimental flux: $16.1\ m^{-2}s^{-1}$
Experimental error: $d\Phi_e = \pm 0.8 m^{-2}s^{-1}$

Experimental flux value is roughly an order of magnitude smaller than expected, likely due to a much smaller angle of acceptance than anticipated, as well as the triple coincidence logic likely cutting out many possible trigger events.

Coherent Electron Cooling: Optimizing Beam Width and Emittance with IMPACT-T

Daemon Howard[1] Vladimir Litvinenko[2,3] Nikhil Bachhawat[2]

[1]Colorado School of Mines [2]Stony Brook University [3]Collider-Accelerator Department, Brookhaven National Laboratory

Motivation

At Brookhaven National Laboratory, the CeC proof-of-principle experiment takes place as a part of the Relativistic Heavy Ion Collider. We aim to validate the ability of CeC through the plasma-cascade microbunching instability (PCI) of the electron beam [1]. CeC uses the electrostatic interaction between electrons and hadrons to drastically reduce the cooling times of accelerators and colliders, with an LHC-like simulation showing a significant decrease from about 13 hours to 1 hour [2].

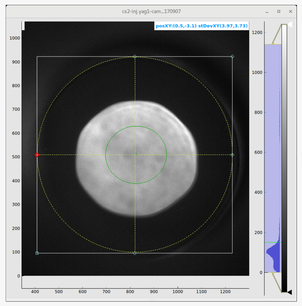

Figure 1: Unfocused beam profile at YAG1.

Background

Particle beams have a property called emittance, the area that the particles take up when plotting the beam in position-momentum phase space. For example, the normalized RMS emittance in the x-direction can be defined as

$$\varepsilon_x = \gamma\beta\sqrt{\sigma_x^2\sigma_{p_x}^2 - \sigma_{xp_x}^2}.$$

From this, a smaller beam has lower emittance. PCI-based CeC requires an electron beam with low emittance. Two factors are considered in this study:

- Solenoid current of Low Energy Beam Transports (LEBTs)
- Solenoid current of the 112 MHz SRF electron gun

To find the optimal currents, we used simulation software known as IMPACT-T. IMPACT-T is a three-dimensional program that tracks relativistic charged particles [3]. We simulated and measured at the sections shown in Fig. 1.

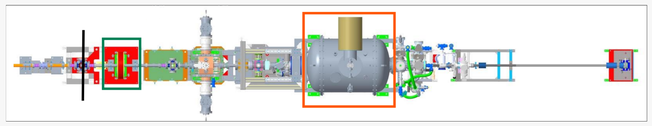

Figure 2: Focused scope of beamline. The orange box encloses the SRF electron gun, the green box encloses the first solenoid in the beamline "LEBT1," and the black line placed at YAG1 shows where we collected data in simulations and experiments.

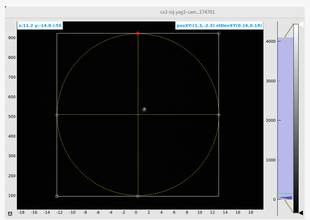

Figure 3: Profile of focused beam at YAG1.

Once optimized, the beam should no longer look like Fig. 1. Rather, it will be smaller and have a low measured emittance, visually resembling the profile in Fig. 3.

Procedure

Using the YAG1 profile monitor, we looked at beam width as a function of LEBT1 and gun solenoid currents, and beam emittance as a function of gun solenoid current. Optimizing beam width and emittance each had different steps:

Beam width:

1. Simulate each current for 800 pC bunches
2. Vary LEBT1 & gun solenoid current
3. Measure average RMS x- and y-widths at YAG1

Beam emittance:

1. Simulate each current with varying size bunches
2. Vary electron gun solenoid current
3. Measure the projected emittance at YAG1

Results

Our work in minimizing beam width found the optimal current settings of $\pm$4.5 A for LEBT1. It also revealed a large mismatch between our expectations and experimental data, seen by the overshooting simulations in Fig. 4 that shift down in Fig. 5. This was caused by our outdated IMPACT-T beamline setup.

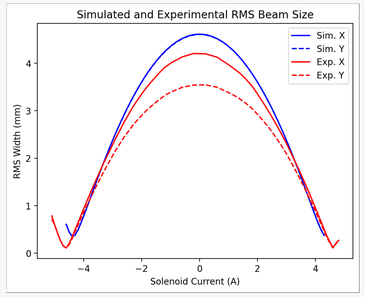

Figure 4: First simulation comparison.

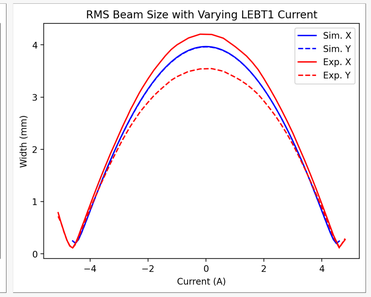

Figure 5: Updated simulation comparison.

0 pC bunches and 800 pC bunches were tested to further verify simulation accuracy. Fig. 6 is unaffected by space-charge, thus simulations should, but do not, match the experiment. Fig. 7 uses the experimental bunch setting. It mostly agrees until about 8.7 A and is optimal around 8.6 A.

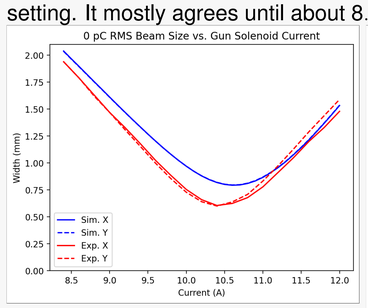

Figure 6: RMS width using 0 pC bunches, shows a mismatch.

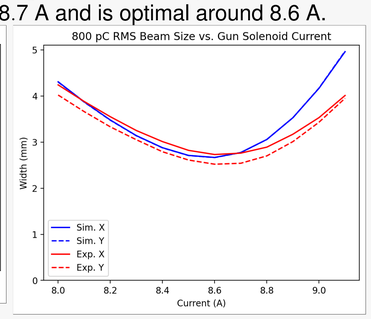

Figure 7: RMS width using 800 pC bunches, shows departure.

The projected X and Y emittance comparisons helped confirm where the minimum emittance is for the 800 pC bunches but were otherwise inconclusive. The large mismatch in Fig. 9 prompted us to see how 0 pC would change given the absence of space-charge, with results shown in Fig. 8.

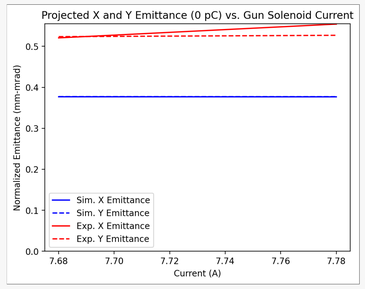

Figure 8: 0 pC simulation comparison.

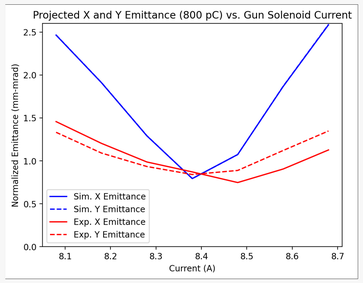

Figure 9: 800 pC simulation comparison.

The deviation from simulations could be caused by:

- Non-uniform beam charge density
- Incorrect photocathode recess measurement affecting electric field strength and focusing in the SRF cavity

Conclusion

After making corrections to the beamline setup, we gained more accurate simulations and found optimal LEBT1 and SRF gun solenoid currents of around $\pm$4.5 A and 8.6 A, respectively. The experimental width measurements aligned with our expectations. The optimal LEBT1 and SRF gun solenoid currents for minimized emittance are still unclear given the large mismatch between simulations and experimental data.

Further work includes generating new electromagnetic field maps for IMPACT-T to account for the new photocathode recess. Another simulation software may also be used to test 0 pC bunches, as IMPACT-T is better suited for space-charge-dominated beams.

References and Acknowledgments

[1] Vladimir N. Litvinenko, Yichao Jing, Dmitry Kayran, Patrick Inacker, Jun Ma, Toby Miller, Irina Petrushina, Igor Pinayev, Kai Shih, Gang Wang, and Yuan H. Wu.
Plasma-cascade instability.
Phys. Rev. Accel. Beams, 24:014402, Jan 2021.

[2] Vladimir N. Litvinenko and Yaroslav S. Derbenev.
Coherent electron cooling.
Phys. Rev. Lett., 102:114801, Mar 2009.

[3] Ji Qiang, Steve Lidia, Robert D. Ryne, and Cecile Limborg-Deprey.
Three-dimensional quasistatic model for high brightness beam dynamics simulation.
Phys. Rev. ST Accel. Beams, 9:044204, Apr 2006.

This material is based on work supported by the National Science Foundation under Grant No. PHY-2243856. I am extremely grateful for this opportunity given to me by the Department of Physics & Astronomy at Stony Brook University. I would like to thank both Vladimir Litvinenko and Nikhil Bachhawat for their immense mentorship, and wish them luck in future endeavors.

Rivet-ing Heavy-flavor-based Analyses from PHENIX

Owen Fiedorowicz

Dr. Roli Esha, Professor Axel Drees

Stony Brook University

IOWA

Abstract

PYTHIA has been one of the more reliable event generators to model relativistic collisions. With an upgrade from the Fortran-based PYTHIA6 to a C++-based PYTHIA8, in addition to new physics processes, newer models based on Multi-Parton Interactions (MPI) have been implemented. In the process, the Monash tune of model parameters for PYTHIA8 works well for LHC energies. However, at RHIC energies, there is a significant difference between event generator models and experimental findings, specifically for heavy flavor production. We approach this problem by using the PROFESSOR tuning method to optimize the model parameters. Writing Rivet analyses to compare PYTHIA8 simulation to data allows PROFESSOR to calculate a goodness of fit function, which is sampled within our parameter space. Using a polynomial fit of the goodness of fit function on the model parameters, the optimal tune is calculated. We hope to use this to tune PYTHIA8 to better model physics at RHIC energies.

Event Generators

Event generators simulate the interactions of particles. They can simulate many different possible processes of particle production.

Event generators are a convenient way to simulate runs of large experiments. In addition, by comparing event generator output to experiment data we can gain an improved picture of the event structure.

A sample event from an event generator. Many processes lead to the blue final particles

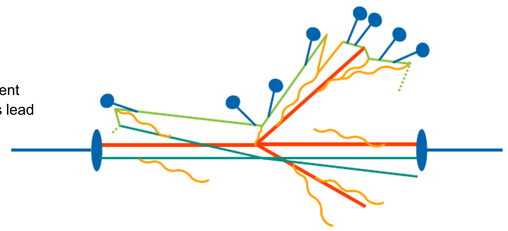

These event generators have free parameters which must be adjusted for the event generator to describe experimental data. Tuning an event generator involves finding a set of model parameters that works well for an experiment.

We work with the event generator PYTHIA8, which has been proven reliable, and the Monash tune works very well for energies found at the LHC.
However, at RHIC energies it does not describe experimental data, specifically for heavy flavor processes.
Our goal is to develop a tune of PYTHIA8 specifically for heavy flavor processes at RHIC.

Rivet

Rivet (Robust Independent Validation of Experiment and Theory) is a system for validating event generators and running analyses on experiments.

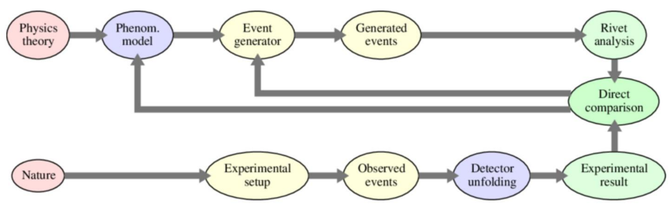

Rivet allows the following:

- Preserving analyses and making them easier to maintain.
- Makes results easier to reproduce
- Gives a common testing ground to compare different generators
- Allows testing of event generators against many different data sets

We will use Rivet to compare PYTHIA8 output to data, in order to tune PYTHIA8.

Comparing Event Generators to Experiment

The invariant cross section is given by:

$$E\frac{d\sigma^3}{dp^3} = \frac{1}{2\pi p_T}\frac{1}{N_{events}}\frac{dN}{dp_T}\sigma_{pp}$$

where σ_{pp} is the cross section for proton-proton inelastic collisions at 200 GeV, which is 42 mb.

Particles in mid-rapidity are typically detected in the experiment. To calculate the total cross section, event generators are used to find the ratio of total cross section, and mid-rapidity cross section.

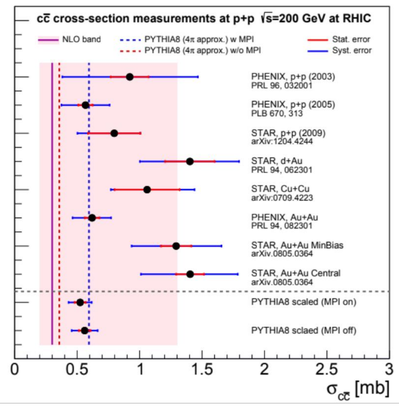

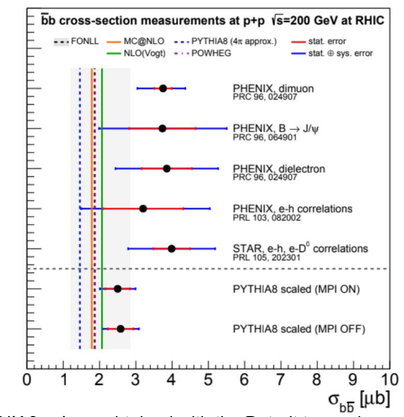

When looking at heavy flavor cross sections at RHIC, PYTHIA8 values, obtained with the Detroit tune, gives smaller results than we find from other models.

Rivet Analyses

Using Rivet, we can write analyses to compare PYTHIA8 output to data for heavy-flavor processes.

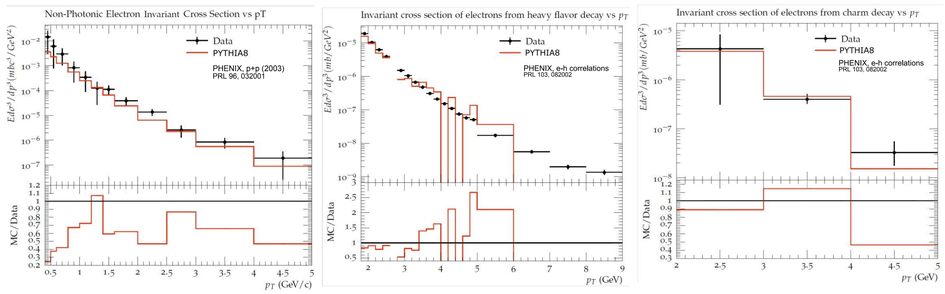

We see a noticeable difference between our output and our data, especially at low p_T. At higher p_T we see much more variance in event generator output, due to low sample size.

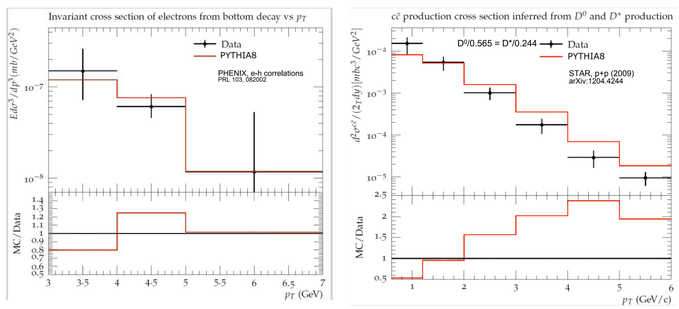

Next Steps: Tuning

For tuning PYTHIA8, we are working in a very large parameter space, with order 10 total potentially relevant parameters. The tuning process becomes an optimization problem and will be done using the PROFESSOR (procedure for estimating systematic errors) method.

First, the PROFESSOR method randomly samples the parameter space and runs the event generator at various points in it. With the output from these points, it runs a polynomial interpolation to approximate generator output.

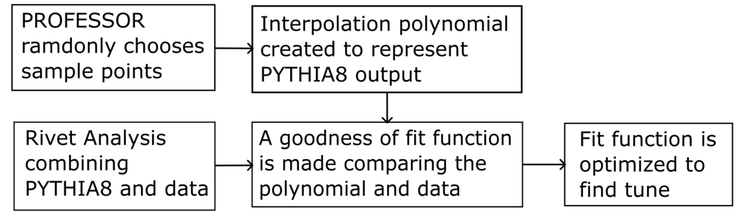

We are using quadratic interpolation, as for each parameter our range is relatively narrowed down. Cubic interpolation is also possible but is significantly more computationally intensive.

Additionally, the parameter space can be split into subspaces to reduce computation time. These subspaces are optimized individually and later combined.

A goodness of fit function is used to compare the difference between the polynomial and experimental data. There are many functions that can be used for this, one of which is a χ^2 fit:

$$\chi^2(p) = \sum_o \omega_o \sum_b \frac{(f^{(b)}(p) - R_b)^2}{\Delta_b^2}$$

where ω are our weights, b is our bin, f(p) is our polynomial, R is our data, and Δ is the uncertainty.

The goodness of fit function is then optimized numerically, and the results are checked.

Summary and Thanks

We have developed Rivet analyses to compare event generator output and experimental data for heavy-flavor contributions. With these we will use the PROFESSOR tuning method to optimize model parameters for PYTHIA8.

I would like to thank Dr. Roli Esha and Professor Axel Drees for mentoring me on this project.

References

Aguilar, Manny Rosales, et al, PYTHIA 8 underlying event tune for RHIC energies, Physical Review D 105 (2022).

Bellm Johannes, Gellersen Leif, High dimensional parameter tuning for event generators, The European Physics Journal C (2019).

Bierlich, Christian, et al, Confronting experimental data with heavy-ion models: Rivet for heavy ions, The European Physics Journal C (2020).

Buckley, Andy, et al, Systematic event generator tuning for the LHC, The European Physics Journal C (2009).

PHENIX Collaboration, Measurement of Bottom versus Charm as a Function of Transverse Momentum with Electron-Hadron Correlations in p+p Collisions at sqrt(s)=200 GeV, Physical Review Letter 103 (2009).

PHENIX Collaboration, Single Electrons from Heavy Flavor Decays in p+p Collisions at √s = 200 GeV, Physical Review Letter 96, 032001 (2006).

Plätzer, Simon, Event Generators and Resummation, University of Graz.

STAR Collaboration, Measurements of D0 and D* Production in p+p Collisions at √s = 200 GeV, Physicsl Review D 86 (2012).

Studies in Saturated Absorption Spectroscopy and its Applications to Optical Force Experiments

Megan Ferland[1] Elise Boria[2] Harold Metcalf [2] Alessandro Tripoli[2]

[1]Colby College [2]Stony Brook University

Abstract

Saturated Absorption Spectroscopy (SAS) is a technique used to extract a precise transition frequency between atomic states that reduces Doppler broadening. Thus, a laser can be locked to a single atomic frequency.

Background

- **Doppler Broadening** is the widening of spectral lines due to the random motion of atoms in a gas. The atoms don't travel in one uniform direction, resulting in a wide frequency range. Doppler broadening is typically two orders of magnitude larger than a spectral line's natural line width.

$$f_{Doppler} = (\frac{v}{c}) f_{Optical}$$

- **Saturation** occurs when a material is inundated with light such the material no longer responds to additional stimuli.

SAS Overview

SAS aims to generate a high-resolution absorption profile of spectral lines. The SAS technique overcomes Doppler broadening by using a beam that saturates the atoms with light (pump beam) so that no absorption occurs for atoms that have no Doppler shift relative to the second beam (probe beam).

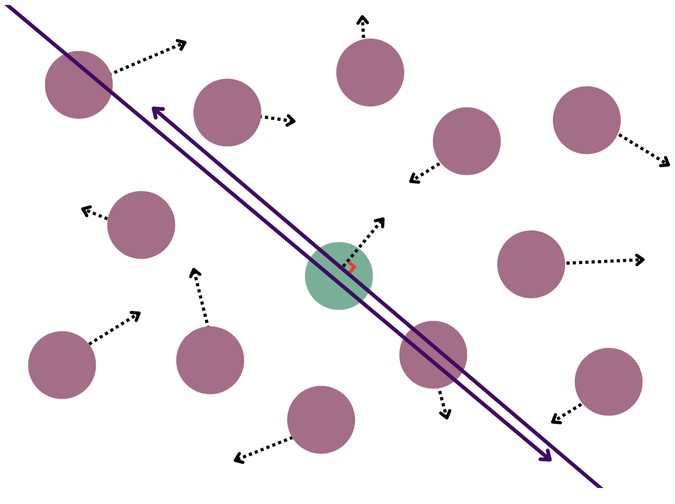

Figure 1. Atoms moving perpendicular to the beams experience no Doppler shift, relative to them. These are the atoms that absorb probe light.

SAS Setup

- **Two counter-propagating beams** that stem from the same laser enter the cell of metastable helium atoms
- **Strong pump beam** drives the cell with excess light, saturating the atoms
- **Weak probe beam** moves through the cell on the same plane, and atoms moving perpendicularly to both beams transmit light as a narrow signal.

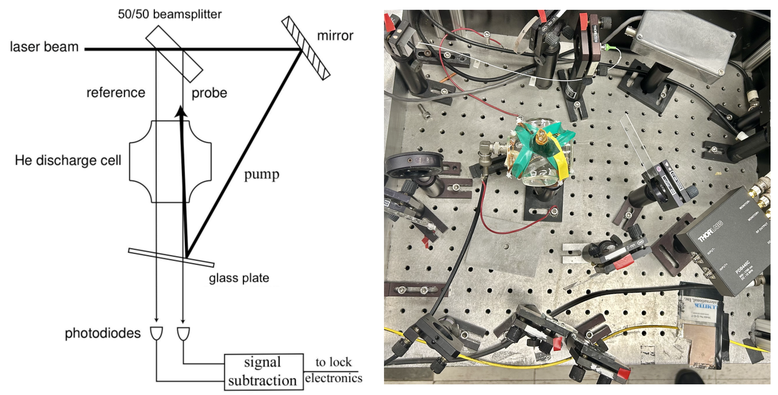

Figure 2. Infrared SAS setup (schematic and lab view) [4]

Resulting Signal

The absorption profile when there is no pump beam present is shown to have a wide Doppler width. When there is a pump beam, there is a spike at the resonant frequency because atoms with no Doppler shift relative to the probe beam are not able to absorb. When we subtract the two plots, we obtain a singular narrow spectral peak.

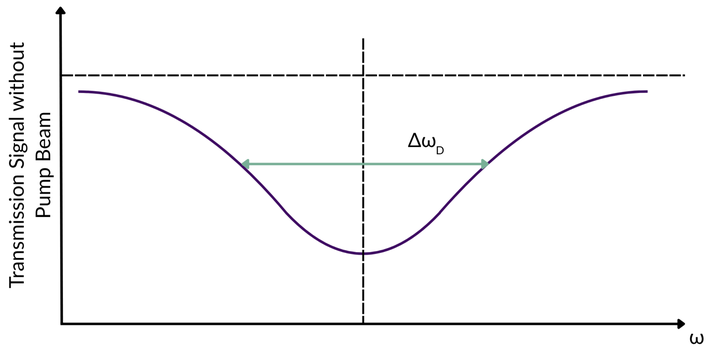

Figure 3. Absorption spectra without the pump beam [4]

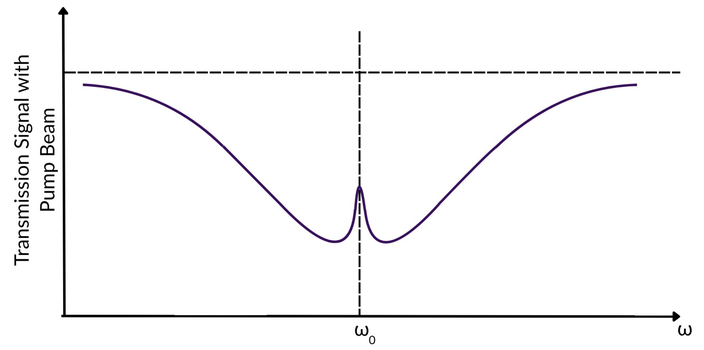

Figure 4. Absorption spectra with the pump beam [4]

Application: Optical Force Experiments

Conservation of momentum deflects atoms when periodic pulse sequences are applied. By stimulated emission, which occurs when light collides with an excited atom, additional light is produced that's moving with the same direction and energy. Optical forces have the capacity to move matter in a precise manner. SAS ensures that the frequency of the incoming beam is stabilized, allowing for further refinement of its application.

Conclusion

With SAS's ability to effectively stabilize a laser to a specific transition frequency, it has numerous applications in optical force experiments, including ongoing ARP and STIRAP projects.

Acknowledgments

Thank you to Dr. Harold Metcalf for his mentorship and engaging teachings throughout the REU. Thank you to Alessandro Tripoli and Adam Jenkins for their guidance. This material is funded by the NSF REU Grant No. PHY-2243856.

References

[1] Brian Arnold.
Velocity dependence of the adiabatic rapid passage force in metastable helium.
Stony Brook University Doctor of Philosophy Dissertation, 2019.

[2] James C. Bergquist.
Doppler-free spectroscopy.
Experimental Methods in the Physical Sciences, 29B, 1996.

[3] X. Miao et al.
Strong optical forces from adiabatic rapid passage.
Phys. Rev. A 75, 011402(R), 2007.

[4] Xiaoxu Lu.
Excitation of helium to rydberg states using stirap.
Stony Brook University Graduate School Thesis, 2011.

[5] Peter van der Straten and Harold Metcalf.
Atoms and Molecules Interacting with Light: Atomic Physics for the Laser Era.
Cambridge University Press, 2016.

Strong Lensing Validation with the Vera C. Rubin Observatory

Mia LaMontagne[1]
University at Albany[1]

Dr. Simon Birrer[2]
Stony Brook University[2]

MOTIVATION

Figure 1. The Vera C. Rubin Observatory, located on the El Peñón peak of Cerro Pachón in Chile. [1]

The Vera C. Rubin Observatory's ten year long Legacy Survey of Space and Time (LSST) will utilize a 8.4-m Simonyi Telescope and 3.2-gigapixel, 9.6 deg² camera to take hundreds of exposures of a ~18,000 deg² sky area. This unprecedented depth and coverage will enable innovative studies of cosmological phenomena, such as strong gravitational lensing. However, the first data release was captured using a lower resolution Commissioning Camera, which covers a limited sky area at a shallow depth. This limits the likelihood of observing real strong lensing, so we simulate it by inject background galaxies, lensed by mass models of real ellipticals, into our cutout images. These realistic injections will aid in preparing for true strong lensing analysis in future LSST data.

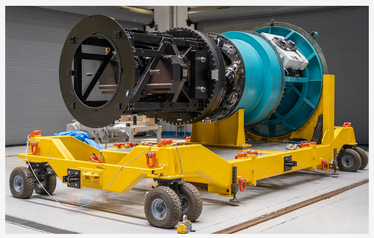

Figure 2. The LSSTComCam. [2]

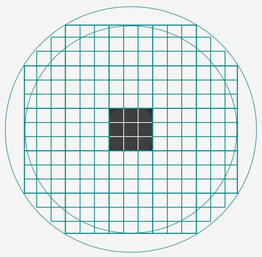

Figure 3. The field of view of the ComCam compared to the full LSST camera. [3]

BACKGROUND

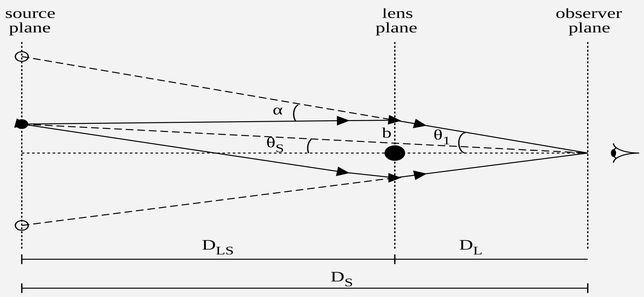

Gravitational lens geometry: α deflection angle; β true source angle; θ lensed image angle; D_l, D_s, D_{ls} angular-diameter distances to lens, source, and between them. [4]

- Gravity from a massive foreground object curves spacetime, bending and magnifying background light into arcs, rings, or multiple images.
- We focus on massive elliptical galaxies as their large mass is centrally concentrated, producing large Einstein radii and bright arcs, making these lenses the easiest to spot and model.

METHODOLOGY

Elliptical Galaxy Extraction

- Analyzed all known galaxies in DP1 release with needed photometry and shape columns for subsequent cuts:
    1. **Bulge Dominant:** Kept galaxies with **bulge-to-total ratio ≥ 0.5** to favor early-type elliptical morphologies.
    2. **Bright:** Required **i-band Sérsic magnitude < 21.0** to select luminous, and subsequently hence high-mass, galaxies.
    3. **Large size:** Required with **Sérsic effective radius ≥ 25 pixels** to bias toward extended, massive galaxies.

Cutouts and Source Galaxy Injection with SLSim

- We produce deep coadd cutout images of each candidate galaxy in the **i-band**.
- We generate a simulated background galaxy and lens it using a mass model derived from the real foreground galaxy [5].
- Simulations are then convolved with real DP1 PSFs and noise injected into the real deep-coadd cutout.

RESULTS

i-band Coadd at RA=58.8707, Dec=-49.2713

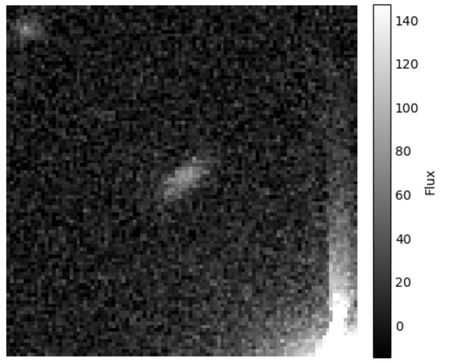

i-band Coadd at RA=49.8601, Dec=-25.4592

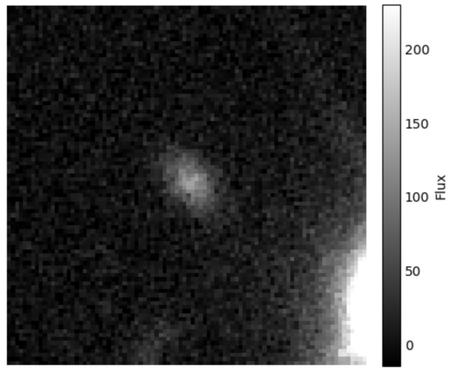

Figures 4 & 5. i-band Deep coadd cutout images of potential massive elliptical galaxies captured by the Vera C. Rubin Observatory.

i-band Coadd at RA=58.8707, Dec=-49.2713 With Source Injection

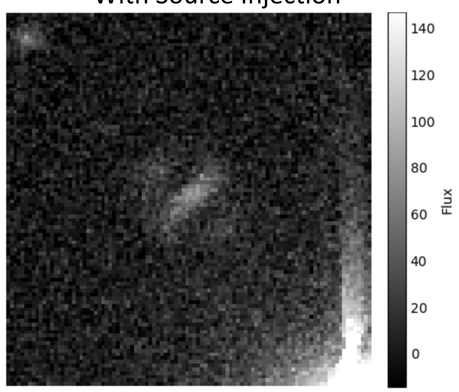

i-band Coadd at RA=49.8601, Dec=-25.4592 With Source Injection

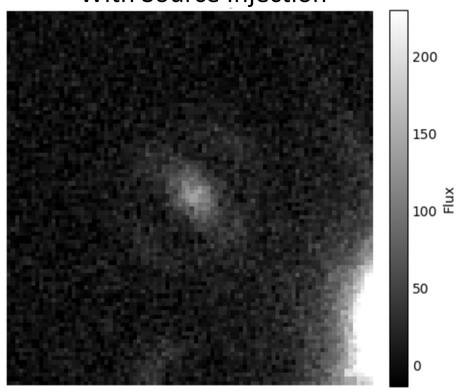

Figures 6 & 7. i-band Deep coadd cutout images of potential massive elliptical with simulated lensed source galaxies injected in.

CONCLUSIONS

Elliptical Galaxy Sample Yield

- **1,374 of 255,525 galaxies** matched our criteria for ellipticity, visualized in deep coadd images.

Realistic Strong Lensing Visualization

- We generated simulated source-deflector systems modeled after observed galaxies.
- This produced realistic strong lensing morphology, matching the matching the PSF noise characteristics of true Rubin DP1 cutouts.

FUTURE WORK

Preparing for Future Data Releases:

- Visual analysis of the simulated lens system allows for training to better identify strong lensing in the complete LSST survey.

Source Galaxy Characterization via Simulations

- Simulations quantify lensing and observational biases, enabling recovery of true source sizes, fluxes, and morphologies.
- How well morphological features, such as rings or arcs, survive lensing and reconstruction informs expectations for real source imaging.

REFERENCES

1. RubinObs/NOIRLab/SLAC/NSF/DOE/AURA/B. Quint. *Gallery.* Vera C. Rubin Observatory, 2022
2. RubinObs/NOIRLab/SLAC/NSF/DOE/AURA/A. Pizarro D. *Gallery.* Vera C. Rubin Observatory, 2024
3. Wikimedia Commons. *Gravitational lens geometry, 2012*
4. NSF–DOE Vera C. Rubin Observatory. *Single-raft LSSTComCam position*. The Vera C. Rubin Observatory Data Preview 1 (RTN-095), 2025
5. A versatile strong-lensing simulation library used throughout this work. Contributions are welcome at the GitHub repository.

ACKNOWLEDGMENTS

This work is supported with funding from the National Science Foundation under Grant No. PHY-2243856. I would like to thank Dr. Simon Birrer for his support and guidance.

Modeling X-Ray Burst Flame Propagation with Castro and Pynucastro

Isabelle McNulty[1,2], Michael Zingale[1]

[1]Stony Brook University [2]University of Massachusetts Amherst

X-ray bursts (XRBs) are thermonuclear explosions on the surface of accreting neutron stars. The aim of this research is to follow up on Eric Johnson's paper[1], which simulated and XRB with a 33-isotope reaction network and observed certain elements left behind. We expand on this work by employing larger reaction networks to better capture the nuclear processes. Here, we use the Castro hydrodynamics code coupled with pynucastro-generated reaction networks to model 2D flame propagation in mixed H/He bursts and explore the effects of network size on flame composition and evolution.

Background

- XRBs are thermonuclear explosions on the surface of accreting neutron stars
- These bursts occur when a critical mass of accreted hydrogen/helium from a binary star ignites, triggering rapid nuclear burning and nucleosynthesis
- The burning front propagates around the star surface
- Light curves show brightness of star over time during an XRB event

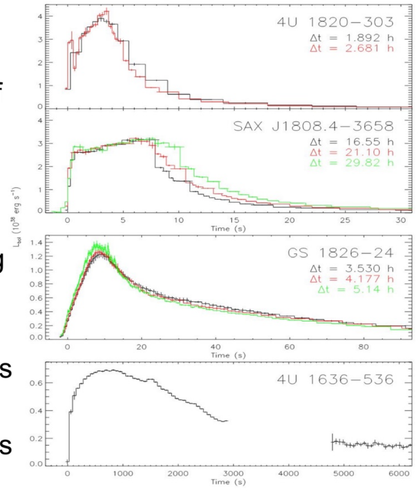

▲Light curves observed by the Rossi X-Ray Timing Explorer (RXTE) of different sources and recurrence times Δt [2]

Methodology

- Started by creating reaction networks in pynucastro
- Used Castro software to solve equations of hydrodynamics for reactive flows via flame_wave setup
- Used mixed H/He at 10% hydrogen and 90% helium
- Ran three simulations of reaction networks of varying size out to 30ms to observe the impact on flame composition and propagation
- 30ms is far enough in to observe an established flame
- Computation done with NERSC supercomputing center
- Visualization using yt utils

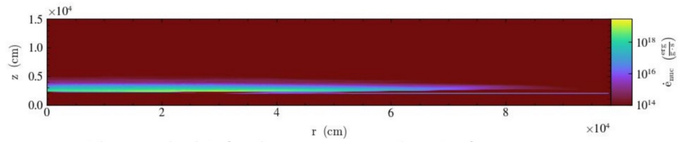

▲An example plot of nuclear energy generation rate of cno-he-burn-33a made using Castro and plotted with yt utils

Conclusion

- Using larger networks reduces artificial bottlenecks as seen in elemental composition pie charts
- Larger reaction networks should be tested and have full simulations run
- As computational barriers are removed these larger networks can be used in 3D simulations
- Additionally, finer resolutions can be explored
- Computational time is a limiting factor in network size. In this simulation the 41 element network simulation took 8630 node hours, ~63% longer than the original 33 element network

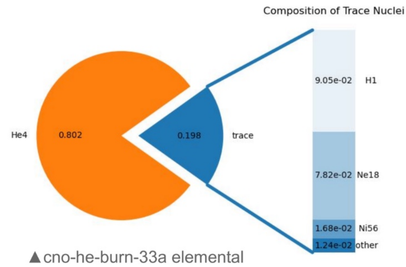

▲cno-he-burn-33a elemental composition after 30ms

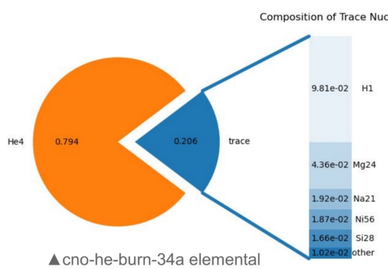

▲cno-he-burn-34a elemental composition after 30ms

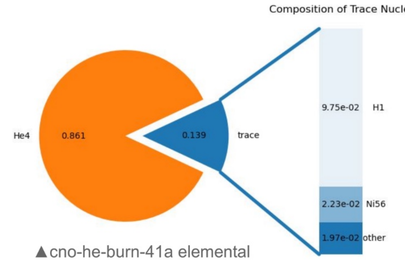

▲cno-he-burn-41a elemental composition after 30ms

Results

- Network graphs produced using pynucastro show mass fraction and approximate reaction rates of the nuclei for each flame at 30ms
- cno-he-burn-33a had large amounts of Na22 on the order of 10^3 left behind, as well as Ne18
- In the cno-he-burn-34a $^{18}Ne(\alpha,p)^{21}Na$ reaction allows with a high approx rate of 0.126
- Proton captures included in the cno-he-burn-40a network removes abundant Na21 and Mg24 present in cno-he-burn-34a through $^{22}Na(p,\gamma)^{23}Mg$ and $^{24}Mg(p,\gamma)^{25}Al$

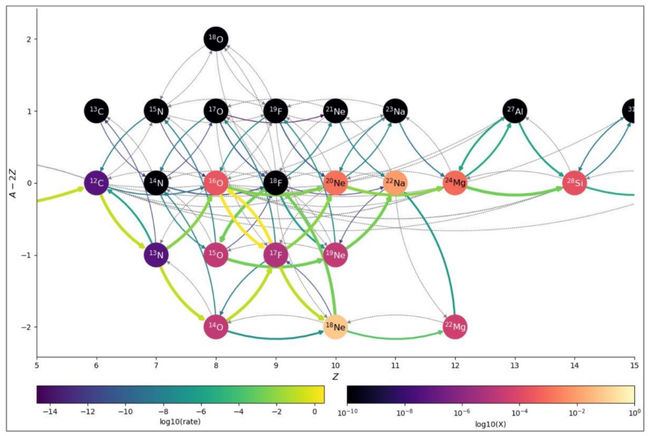

cno-he-burn-33a network with 33 elements at 30ms (original network)

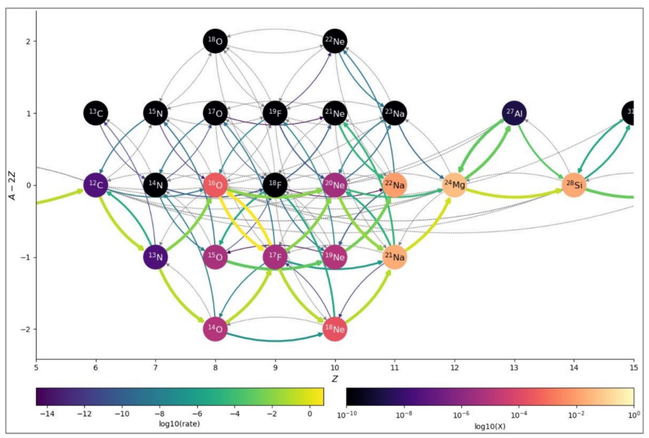

▲cno-he-burn-34a with 34 elements at 30ms

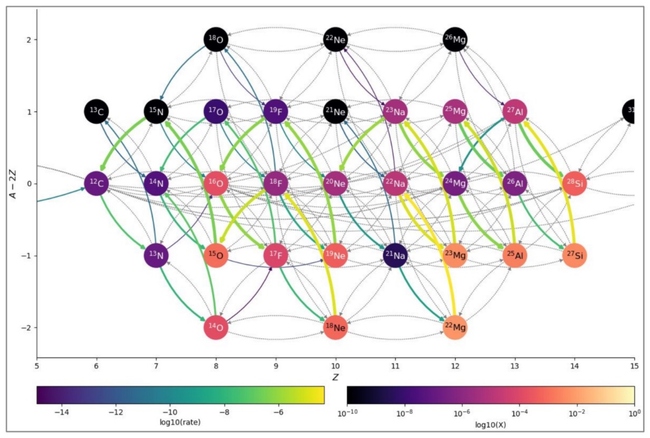

▲cno-he-burn-40a network with 40 elements at 30ms

References

- [1]Johnson, E. T., & Zingale, M. (2025). Multi-dimensional Models of Mixed H/He Flames in X-ray Bursts. arXiv preprint arXiv:2505.13879. https://doi.org/10.48550/arXiv.2505.13879
- [2]Galloway, D.K. & Keek, L. (2017). Thermonuclear X-ray bursts. arXiv:1712.06227. https://doi.org/10.48550/arXiv.1712.06227
- Castro: https://github.com/AMReX-Astro/Castro
- Pynucastro: https://github.com/pynucastro/pynucastro

All code is freely available on Github

Analytic Scaling of the Lensing Tail of the Cosmic Microwave Background Power Spectrum

Megan Schlogl[1,2], Yijie Zhu[1], Vivian Miranda[1]

1. Stony Brook University, 2. Rensselaer Polytechnic Institute

The CMB Power Spectrum

The Cosmic Microwave Background (CMB) is the photons from the surface of last scattering. In this signal, we see anisotropies that correspond to over- and under-densities from the primordial Universe. This can be represented by the temperature-temperature correlation function C_ℓ^{TT}, which quantifies the similarity of the temperatures of the CMB at two points in the sky separated by a given scale.

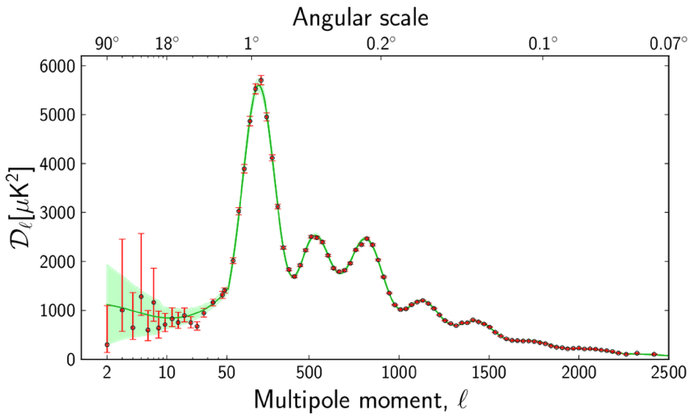

Image from [3]. The scaled CMB power spectrum $D_\ell = \ell(\ell+1)C_\ell/2\pi$

Gravitational Lensing

The force of gravity, such as from a cluster of galaxies, bends spacetime, thus changing the path light travels. We see light coming from a different place than it really is, causing for example a smearing in the CMB signal. This effect dominates at large ℓ, or small scales.

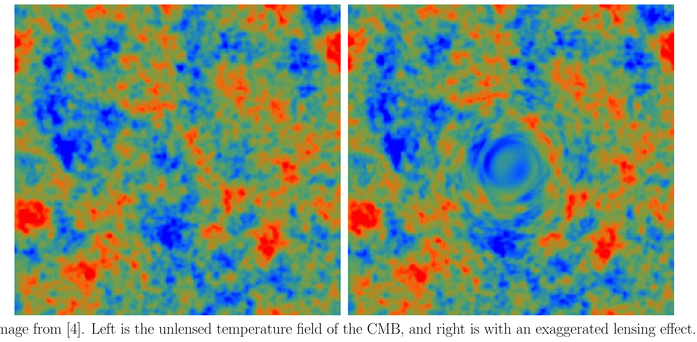

Image from [4]. Left is the unlensed temperature field of the CMB, and right is with an exaggerated lensing effect.

Motivation

Markov Chain Monte Carlo (MCMC) chains are used to infer cosmological parameters from a dataset, but as the precision of future measurements demands more extensive analysis, they are becoming increasingly computationally expensive. Using machine learning to emulate CMB power spectra from CAMB data can reduce computation time for MCMC chains.

In this project, we analytically scale the CMB lensing tail. By pre-processing in this way, we can reduce the span of the data vectors, hopefully decreasing training time.

Cosmological Parameters

Cosmological parameters describe the evolution and current state of the Universe. In this project, we examined the effect of gravitational lensing on the CMB considering five parameters: the Hubble constant H_0, the baryon density $\Omega_b h^2$, the cold dark matter density $\Omega_c h^2$, the power of the primordial curve perturbations A_s, and the scalar spectrum power-law index n_s. We explored the following parameter space:

Ranges for Cosmological Parameters					
	H_0 (km/s/Mpc)	$\Omega_b h^2$	$\Omega_c h^2$	$a = \ln(A_s \times 10^{10})$	n_s
Minimum	50	0.007	0.04	1.61	0.8
Fiducial	80	0.0224	0.12	3.043	0.965
Maximum	67.4	0.035	0.23	3.6	1.2

Fitting Model & Optimization

The lensing tail is defined as the lensed power spectrum divided by the unlensed power spectrum: $L(\ell) = \frac{C_\ell^{\text{lensed}}}{C_\ell^{\text{unlensed}}}$. We model the lensing tail as:

$$L(\ell) = 1 + w(\ell)\left[\beta_1 \cdot \left(\frac{\ell}{\beta_2}\right)^{\alpha} - 1\right]$$

$$w(\ell) = \frac{1}{1 + e^{-(\ell-\beta_3)/\beta_4}}$$

where $w(\ell)$ is a weighting function. Here each of the parameters, β_1, β_2, β_3, β_4, and α, is allowed to be a function of the cosmological parameters centered around the fiducial values (except H_0).

Comparison with CAMB Lensing Tail

To create a fit, we employed linear and quadratic regression, using the Levenberg-Marquardt algorithm. For example, for the behavior of β_1 for changes in n_s is:

$$\beta_1(n_s) = b_1\left(\frac{n_s}{0.965} - 1\right) + b_2\left(\frac{n_s}{0.965} - 1\right)^2$$

We developed a fit using 600 random parameters in the selected range, with the lensing tail behavior found using CAMB. The fit was trained to each parameter in isolation, then in pairs, then altogether.

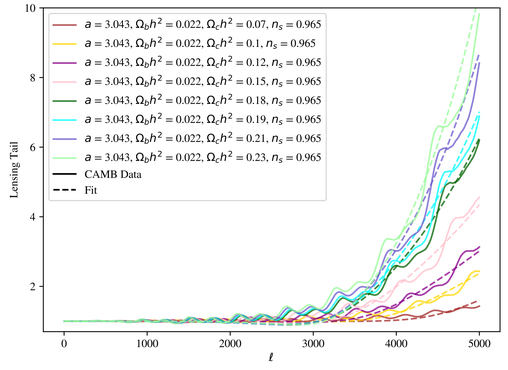

A plot of the fit for varied $\Omega_c h^2$. As shown, the fit captures the order of magnitude of the tail, not its oscillatory behavior.

The overall mean error compared to CAMB for the 600 cosmologies used for training was 12.3%. The error was low near the fiducial cosmology.

Effect of Rescaling

Scaling the lensing tail decreased the span of the vectors:

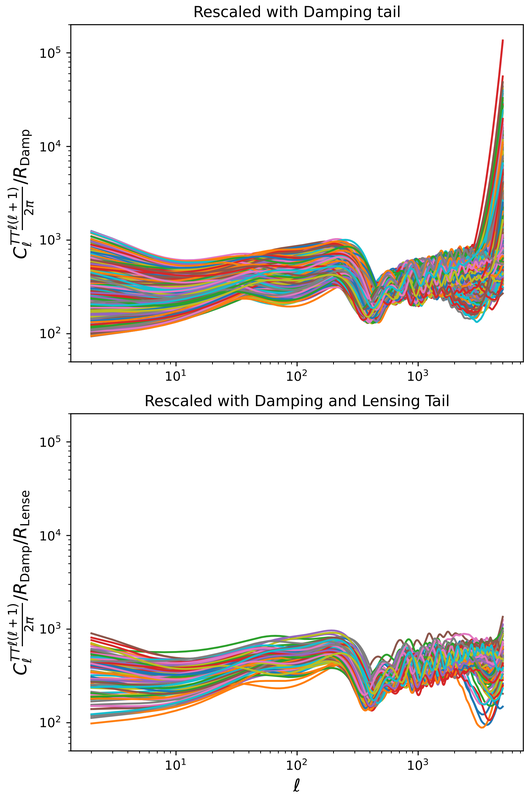

A plot of CAMB data before and after dividing by the equation found for the lensing tail.

Conclusion

We have found that we can model the scale of the CMB lensing tail for pre-processing in machine learning.

In the future, we will expand this study by using machine learning algorithms to create a more precise fit as well as expand the parameter space.

Bibliography & Acknowledgments

This material is based upon work supported by the National Science Foundation under Grant No. 2243856. Any opinions, findings, and conclusions or recommendations expressed in this material are those of the author(s) and do not necessarily reflect the views of the National Science Foundation.

References

[1] Zhu, Y., Saraivanov, E., Kable, J. A., et al. 2025, arXiv:2505.22574. doi:10.48550/arXiv.2505.22574

[2] Nijjar, A. 2025

[3] Durrer, R. 2008, doi:10.1017/CBO9780511817205

[4] Hu, W. & Okamoto, T. 2002, ApJ, 574, 2, 566. doi:10.1086/341110

Sub-GeV atmospheric ν energy reconstruction in LArTPCs for DUNE

Sanskar Jain[1]
[1]The University of Texas at Austin

Introduction

Neutrinos (ν) are weakly-interacting fundamental particles which oscillate between three 'flavors' – ν_e, ν_μ, ν_τ – as they travel. The extent of the 'mixing' between the three flavors and the rates at which they oscillate is determined by certain parameters – three mixing angles, the three neutrino mass differences, and more.

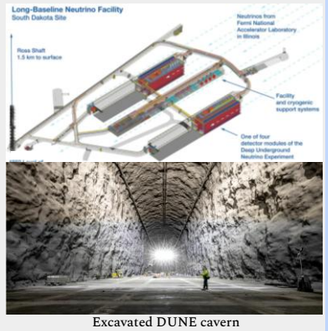

Excavated DUNE cavern

The next-generation neutrino experiment DUNE (Deep Underground Neutrino Experiment) will perform precise measurements of these neutrino oscillation parameters, including the unknown δ_{CP}: the difference in how neutrinos and antineutrinos ($\bar{\nu}$) oscillate (CP violation)[1]. To do so requires determining the energy E_ν of detected neutrinos. So, the DUNE Phase-II Far Detector (FD) will consist of four 17 kt Liquid Argon Time Projection Chamber (LArTPC) modules – tanks filled with liquid argon subjected to a uniform electric field.

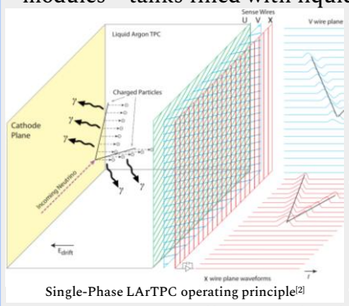

Single-Phase LArTPC operating principle[2]

- When a ν interacts with an Ar nucleus in the tank, its E_ν is distributed among various emitted particles.
- The charged particles deposit their energy by ionizing and exciting Ar atoms along their path.
- The # of collected ionization e^- acts as a measurement of the amount of energy deposited by each particle, from which E_ν can be reconstructed.
- The same is true in principle for the # of scintillation γ, but low photodetector efficiency and coverage have so far made LArTPC light calorimetry infeasible, an issue which the design of the DUNE Phase-II FD aims to resolve. This would provide a second, independent method of estimating E_ν.[4]
- Interactions between cosmic rays and particles in the upper atmosphere are a continuous source of ν with a wide range of E_ν spanning 0.1-100 GeV[3]. However, there is still much work to be done to improve reconstruction methods of ν events at the lower end of that energy range – sub-GeV events.


ProtoDUNE LArTPC[6]

Research Goal

To characterize the performance of charge and light calorimetry in LArTPC in the reconstruction of sub-GeV incident ν energies, as well as explore avenues of ν / $\bar{\nu}$ discrimination.

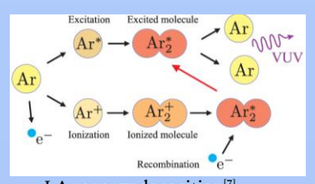

LAr energy deposition[7]

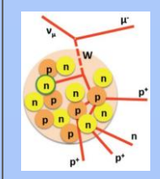
Depiction of FSI[5]

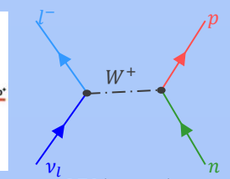

QES interaction

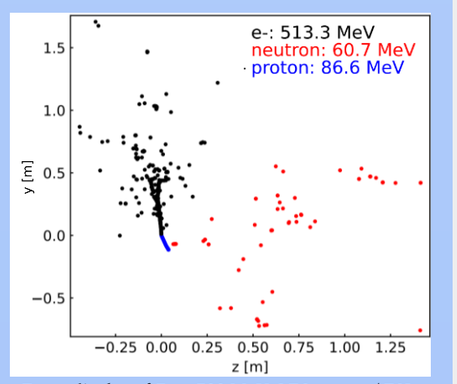

Event display of E_ν = 700 MeV QES event w/ FSI

Methods

The GENIE v3 Monte Carlo neutrino event generator was used to simulate 1000 ν_e-Ar and $\bar{\nu}_e$-Ar charged current interactions each for 10 different values of E_ν from 100 to 1000 MeV. The propogation of and energy deposition by the resultant particles through the LAr was simulated with GEANT4 via the edep-sim package.

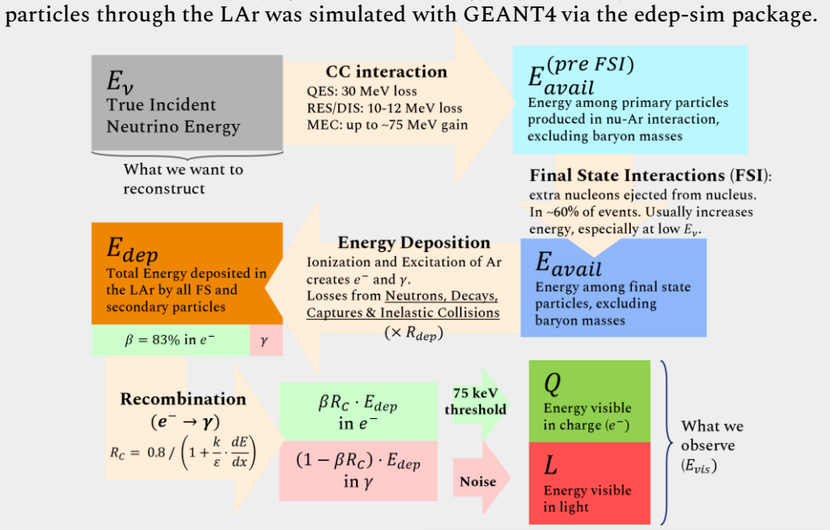

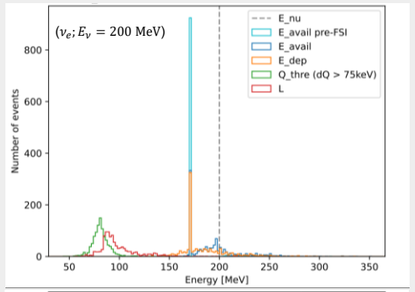

Distributions of E_{avail}, E_{dep}, Q, L for two sub-GeV ν_e event samples

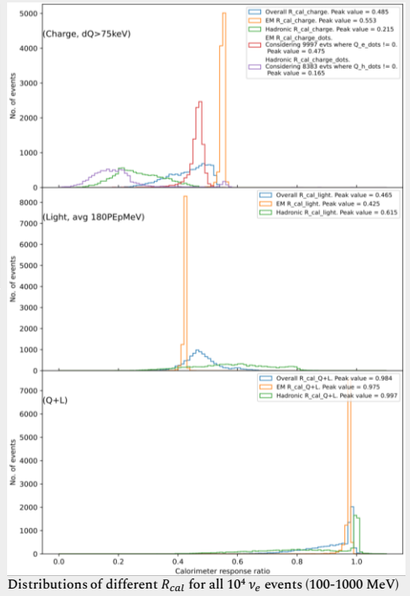

Distributions of different R_{cal} for all 10^4 ν_e events (100-1000 MeV)

$$R_{cal} = \frac{E_{vis}}{E_{avail}} = \frac{E_{vis}}{E_{dep}} \cdot \frac{E_{dep}}{E_{avail}} = \begin{cases} \beta R_C \cdot R_{dep} & \text{(charge)} \\ (1 - \beta R_C) \cdot R_{dep} & \text{(light)} \end{cases}$$

Both R_C and R_{dep} vary for different particles at different energies, especially within the hadronic component, causing event-by-event fluctuation in R_{cal}.

Still, E_ν can be approximately reconstructed by dividing out the measured E_{vis} distribution by the peak value of the corresponding R_{cal} distribution – at least scaling the peak in E_{vis} to match the peak in E_{avail} – before adding back the constant ~30 MeV nucleon removal energy.

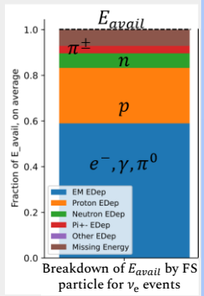

Breakdown of E_{avail} by FS particle for ν_e events

$$L1 = \frac{L}{R_{cal(light)}} \qquad Q1 = \frac{Q}{R_{cal(charge)}}$$

$$Q2 = \frac{Q_e}{R^e_{cal(charge)}} + \frac{Q_h}{R^h_{cal(charge)}} \qquad Q3 = E^{tracks}_{dep} + \frac{Q^{dots}_e}{R^{e,dots}_{cal(charge)}} + \frac{Q^{dots}_h}{R^{h,dots}_{cal(charge)}}$$

$$(Q+L)1 = \frac{Q+L}{R_{cal(overall)}} \qquad (Q+L)2 = \frac{Q_e+L_e}{R^e_{cal(overall)}} + \frac{Q_h+L_h}{R^h_{cal(overall)}}$$

Results

Reconstructed Energy (E_{rec}) distributions for two sub-GeV ν_e event samples

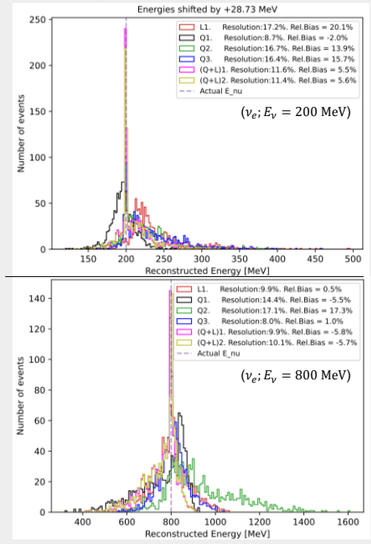

Biases and resolutions of E_{rec} distributions for all 10 ν_e samples

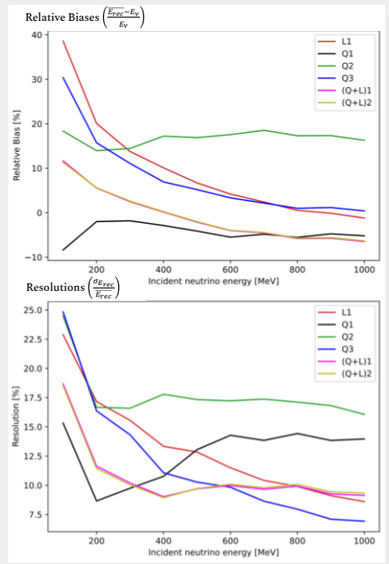

Future Work

Measuring the degree of CP violation in neutrino oscillation (δ_{CP}) requires being able to discriminate between ν and $\bar{\nu}$ in the detector. Specifically, achieving ν_e / $\bar{\nu}_e$ separation would provide the strongest δ_{CP} resolving power.

Comparing the frequencies of various event topologies among the generated 10^4 ν_e and $\bar{\nu}_e$ events reveals significant differences, since the pre-FSI nucleon (surviving in ~30% of events) is always a proton if ν_e and a neutron if $\bar{\nu}_e$. However, this ignores systematics e.g. threshold effects which can obscure particle identification. More importantly, the statistics of different event topologies would depend heavily on the specific FSI model used by the generator and may not correspond well with reality.

FS topology	ν_e	$\bar{\nu}_e$
1p0n0π	2865	0
1pXn0π	2258	2571
0pXn0π	76	4028
π+ present	917	41
π- present	57	882

- No significant difference between track multiplicities in ν_e vs $\bar{\nu}_e$ events was found, likely since FSI produce extra protons and neutrons with about equal likelihood.
- While the 'blip' multiplicity distributions are more distinct, they still cannot provide any definitive separation.
- Separation based on the fraction of the visible energy in the hadronic system is another promising angle.

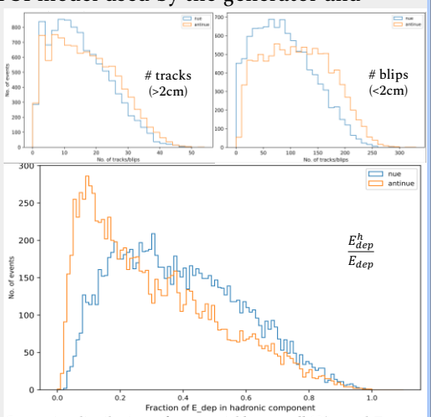

Comparing distributions of some variables over all 10^4 ν_e and $\bar{\nu}_e$ events

Acknowledgements

I would like to thank Dr. Riccio and Dr. Shi for all their mentorship and guidance on this project, as well as the Stony Brook REU program for the opportunity.

References

[1] A. Abed Abud et al 2024 JINST 19 P12005
[2] B. Abi et al 2020 JINST 15 T08010
[3] DUNE Collaboration. *Reconstruction of atmospheric neutrinos in DUNE's horizontal drift far detector module*
[4] Ning et al *Self-compensating light calorimetry with liquid argon time projection chamber for GeV neutrino physics*
[5] J Libo. *GENIE: Neutrino Interaction Modeling and Tuning*
[6] W Kevin *Deep Underground Neutrino Experiment (DUNE): Prospective Physics Program and Status*
[7] B Vittorio *The ArDM project: A liquid argon TPC for dark matter detection*

Using Machine Learning to Improve Dilepton Signal Extraction

Gabriel Rodriguez, Bishoy Dongwi, Charles Naïm
Department of Physics and Astronomy

Introduction

Dilepton production within p+p collisions are the result of several different processes: the Drell Yan process, J/ψ, Υ, open charm, open bottom, and light meson decays. Isolating individual processes to study is difficult due to signal overlap. In response to this problem, machine learning techniques can be used to improve signal-to-background data extraction. By training a machine learning model to categorize dilepton pairs, researchers can easily isolate individual processes despite the signal overlap. These new techniques will provide researchers with more accurate datasets, helping them to study these processes further.

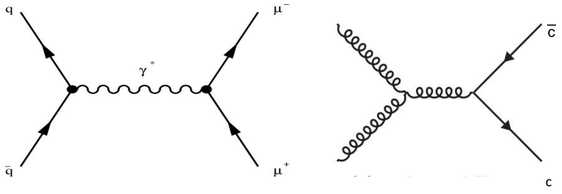

Simulation

Before a machine learning model can make predictions, it must first be trained on a dataset. The training datasets were generated using PYTHIA 8.315 to simulate p+p collisions at a center-of-mass energy of √s = 200 GeV.

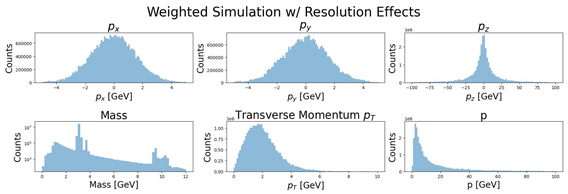

Two datasets were generated using PYTHIA: one for training and one for testing. The training dataset was made by individually simulating each process, normalizing their contributions, and then combining the results to create a balanced dataset in which all processes are equally represented. In contrast, the test dataset was generated by simulating all processes simultaneously, creating a more realistic result that offers a more accurate assessment of the model's performance.

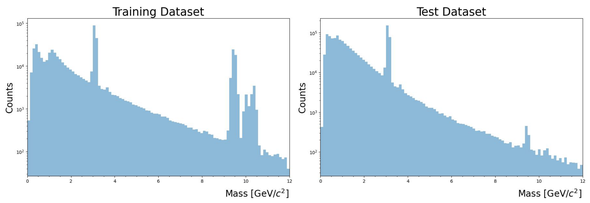

Methodology

Initial attempts to use machine learning for classification involved a neural network; however, the neural network was inefficient due to its long runtime and poor accuracy. The approach was then changed from using a neural network to using gradient boosting with the XGBoost Python library. Gradient boosting is designed and optimized for classification, using iteration and several weak decision trees to make predictions. Shifting to gradient boosting increased accuracy from 20% to 90% and reduced runtime significantly.

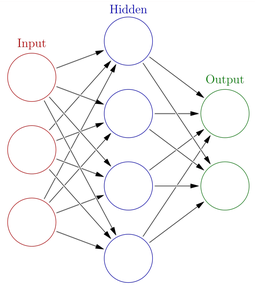

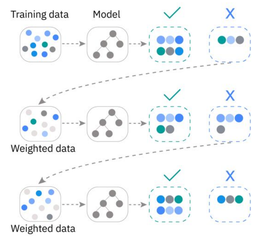

Initial results showed that the model concentrated on the most frequent processes only, leading to lower accuracy for less represented ones. To address this, the training dataset was constructed with equal proportions of dilepton pairs from each process, aiming to promote balanced predictive performance. The test dataset, by contrast, was designed to reflect a realistic distribution of events, providing a more accurate assessment of the model's effectiveness under practical conditions.

	precision	recall	f1-score	support
Drell Yan	0.69	0.68	0.69	30028
J/ψ	0.94	0.99	0.96	39755
Υ	0.96	0.99	0.98	17945
Open Charm	0.47	0.44	0.45	26216
Open Bottom	0.63	0.62	0.63	23892
CB	0.75	0.76	0.76	29788
accuracy			0.76	167624
macro avg	0.74	0.75	0.74	167624
weighted avg	0.75	0.76	0.75	167624

Model Training Results

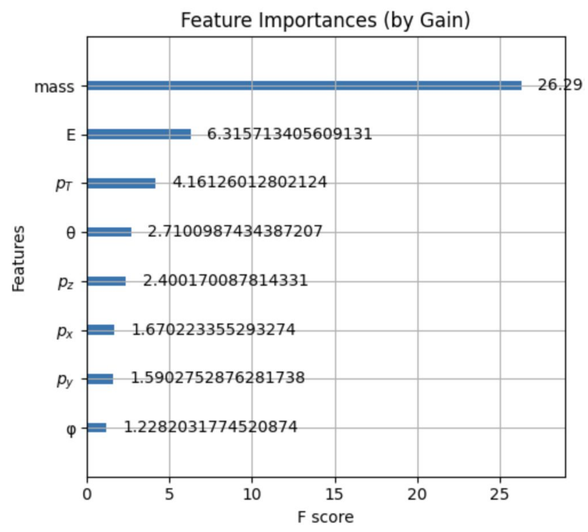

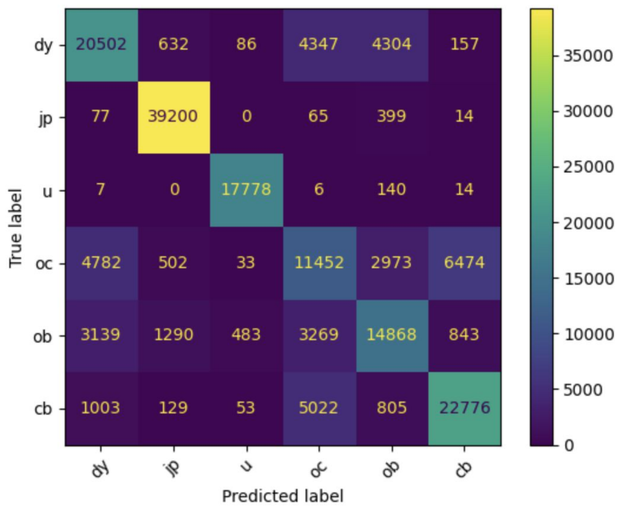

Model Prediction Results

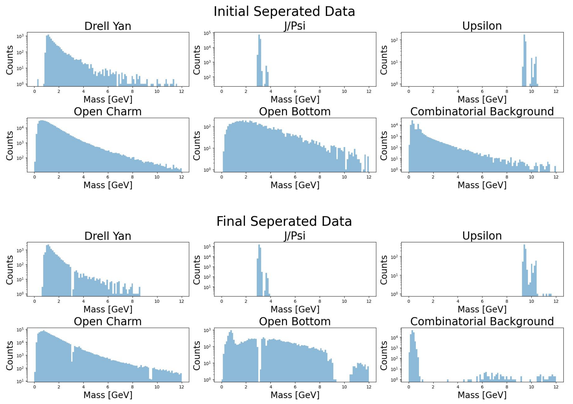

The trained model is able to predict the process responsible for creating each dilepton pair, and classify the pairs by process for further analysis. Pictured above are the dilepton pairs plotted by process, first separated manually for comparison, and below separated by the model using its predictions.

Conclusion

Preliminary findings demonstrate that machine learning techniques can be effectively applied to signal processing, particularly for distinguishing signal data from background noise. The model developed and employed here effectively isolates signals across different processes, demonstrating reliable performance in signal extraction.

Test Accuracy: 0.8266

	precision	recall	f1-score	support
Drell Yan	0.31	0.31	0.31	13583
J/ψ	0.94	0.98	0.96	225621
Υ	0.60	0.94	0.74	586
Open Charm	0.84	0.91	0.88	800535
Open Bottom	0.19	0.23	0.21	12013
CB	0.58	0.33	0.42	180031
accuracy			0.83	1232369
macro avg	0.58	0.62	0.59	1232369
weighted avg	0.81	0.83	0.81	1232369